PCCP

Relationship Between Ferromagnetism and Formation of Complex Carbon Bonds in Carbon Doped ZnO Powders

Journal:	*Physical Chemistry Chemical Physics*
Manuscript ID	CP-ART-03-2019-001277.R1
Article Type:	Paper
Date Submitted by the Author:	28-Mar-2019
Complete List of Authors:	Beltran, Jailes; Universidad de Cordoba Barrero, Cesar; Univeridad de Antioquia Punnoose , Alex ; Boise State University

Relationship Between Ferromagnetism and Formation of Complex Carbon Bonds in Carbon Doped ZnO Powders

Jailes J. Beltrán [1]*, Cesar A. Barrero[2] and Alex Punnoose[3] (†)

[1]*Facultad de Ciencias Básicas, Departamento de Química, Universidad de Córdoba, Carrera 6 No. 77-305, Montería, Colombia.*

[2]*Grupo de Estado Sólido, Facultad de Ciencias Exactas y Naturales, Universidad de Antioquia – UdeA, Calle 70 # 52-21, Medellín, Colombia.*

[3]*Department of Physics, Boise State University, Boise, Idaho 83725-1570, USA.*

**Corresponding Author E-mail: jailesbeltran@correo.unicordoba.edu.co, jjbj08@gmail.com*

† R.I.P. Deceased July 23, 2016.

ABSTRACT

We have investigated the possible relationship between defects, carbon bonds and the associated magnetic properties of carbon doped ZnO powders with nominal carbon intentional concentrations of 0, 1, 3, 5, 8 and 10 mol %. The samples were prepared by mechanical milling assisted by solid state reaction and carefully characterized using different techniques. X-ray diffraction and micro-Raman analysis revealed structural changes below and above the nominal carbon doping concentration of 3 mol % along with formation of intrinsic defect complexes. It was found that the oxygen, zinc content and the band gap of ZnO gradually decreases with increasing carbon content. XPS studies revealed the formation of Zn–O–C and O–C–O bonds and partial substitution of oxygen by carbon, in the form of Zn–C in all samples. When the nominal doping concentration increased above 3 mol %, formation of C–Zn–C bonds was drastically increased. Undoped ZnO sample was diamagnetic and free pure graphitic carbon was paramagnetic, while the 3 mol % carbon doped ZnO sample displayed maximum saturation magnetization. The room temperature ferromagnetism (RTFM) has been ascribed to the presence of Zn–O–C, O–C–O and O–Zn–C bonds, where oxygen atoms may play a crucial role for mediating the long range magnetic interaction. C–Zn–C bonds decrease the saturation magnetization by encouraging antiferromagnetic behavior and the formation of intrinsic defects related with the carbon doping seem to have no influence on the RTFM observed.

Keywords: C–ZnO bulk, Diluted magnetic semiconductor, d^0 Ferromagnetism, XPS, Room temperature ferromagnetism.

1 INTRODUCTION

The search for room temperature ferromagnetism (RTFM) in semiconductor metal oxides such as ZnO has been performed extensively during last two decades. This was based on the prediction by Dietl *et al.*[1] that doping Mn into the nonmagnetic ZnO host could induce ferromagnetic (FM) behavior, while retaining its semiconducting property. Reports on the observation of RTFM in ZnO by doping with 3d transition metals increases daily. In these systems, the origin of this behavior is highly controversial and is still a matter of wide debate. Additionally, it has been a difficult task to completely exclude secondary phases of transitions metal (TM) oxides and to make sure that the observed ferromagnetism really stems from an intrinsic origin, instead of an extrinsic spurious phase. On the other hand, it has been reported that pure ZnO, with different morphologies becomes FM,[2–4] without the presence of any dopant, or when the size of the crystallites is highly reduced.[5] Clearly, these claims suggest that intrinsic defects in ZnO can be the responsible for the origin of this behavior. Therefore, the ferromagnetism has been considered as an universal property of nanoparticles due to the increased presence of defect states and originated from exchange interactions between localized electron spin moments resulting from oxygen vacancies (V_O) at the surfaces of nanoparticles.[6] RTFM in ZnO nanoparticles capped with organic molecules has also been observed. Organic molecules, such as thiol, amine or trioctylphosphine oxide (TOPO), when coated onto ZnO nanoparticles, can modify its electronic structure, giving rise to FM behavior at RT without the need of magnetic dopants.[7,8]

Peng *et al.*[9] have investigated via first principles calculations, the origin of "d^0 ferromagnetism" in ZnO as a prototype material, which does not contain ions with partially filled d or f bands. In their

work, it was shown that the spontaneous magnetization in first row d^0 oxide semiconductors with sufficient holes is an intrinsic property and can be attributed to the localized nature of the 2p states of O. This so called "d^0 ferromagnetism" could be an alternate mechanism for RTFM in non-TM doped ZnO system.

Several recent studies have observed RTFM in non-TM doped ZnO nanoparticles and thin films for which the samples do not suffer from clustering of dopants. FM properties at RT have been reported for B, K, Li, Al and Ga doped ZnO.[10–16] The induced magnetic moment on the oxygen atoms in the nearest neighbor sites to B–Zn vacancy pairs was suggested as responsible for the observed FM behavior in B doped ZnO.[10,11] Unpaired electrons of B–Zn vacancy pairs may cause the polarization of the spin orbital of nearest neighbor oxygen atoms, which provides net magnetic moment for RTFM. Ghosh *et al.*[12] have reported that zinc vacancies (V_{Zn}) might originate the d^0 ferromagnetism in ZnO nanowires. The FM response was found to be enhanced after K doping in the ZnO samples. The incorporation of K in the ZnO lattice might promote the formation of V_{Zn} in the system and introduce holes to stabilize the hole mediated RTFM. In the same way, lithium doping seems to have a similar role in the FM behavior at RT of ZnO nanoparticles as reported by Ullah *et al*.[13] In Al doped ZnO, the physical origin of the induced ferromagnetism was associated with a charge transfer between Zn atoms and adsorbed Al atoms.[14,15,17] In Ga doped ZnO systems the FM signal was attributed to the presence of V_O that act as *F*-centers and leads to the trapping of free electrons.[16]

Among these "d^0 ferromagnetic" systems, carbon doped ZnO has received a great deal of attention because it could be a promising intrinsic diluted magnetic semiconductor[18] with potential light photocatalytic applications.[19,20] Therefore, magnetic properties of carbon doped ZnO have been

investigated experimentally in bulk and in thin films, as well as theoretically.[21–37] Based on literature reports, the role of carbon and oxygen on the origin of RTFM in ZnO is highly debatable as to whether it is due to the presence of impurities, substitution of carbon in oxygen sites or to several intrinsic defects induced by carbon atoms. The origin of the magnetic properties in carbon doped ZnO are not fully understood because of lack of systematic studies on these samples. Thus, this system needs to be further explored and carefully characterized in order to better understand the origin of the observed ferromagnetism and the underlying physics to develop new potential applications. In particular, we need to understand whether the observed ferromagnetism is connected to carbon substituted for oxygen or zinc or if it forms some magnetic defect structures.

In this paper, we investigate the evolution of crystallographic, structural, optical and magnetic properties in carbon doped ZnO bulk samples, with varying carbon concentrations. The goals include studying the effect of introducing and distributing carbon atoms in ZnO and their chemical environment. Possible relations between the defects, carbon bonds, on the one hand, and the magnetic properties, on the other hand, of this system will also be investigated.

2. EXPERIMENTAL DETAILS

Carbon doped ZnO powders were obtained by mechanical ball milling assisted by means of solid state reaction. The samples were prepared to obtain a nominal carbon intentional concentration of 0, 1, 3, 5, 8 and 10 mol %. High purity ZnO (99.9 %) and carbon graphite powder (99.9 %) were mixed as purchased, without further purification, in proper proportion (resulted in samples of about 1.0 g) and hand ground in an agate mortar for half an hour. These powders were milled and subsequently annealed. The mechanical ball milling was carried out in a planetary ball mill Fritsch

Pulverisstte 5 by using agate jars of 250 mL with 6 balls of 12 mm diameter made of the same material. All millings were carried out in argon atmosphere at 250 rpm for 6 h. Each sample was milled for intervals of 1 h and break periods of 30 min up to completion of the desired milling time. The mixture obtained was milled again at 100 rpm for 1 h, in air atmosphere, to obtain a homogenous powder. The precursors obtained were pressed into discs and then annealed at 950 ^{o}C for 45 min, in an electric muffle furnace, heating at 5 ^{o}C/min and slowly cooled at 2 ^{o}C /min in argon flow. Finally, these pellets were annealed at 400 ^{o}C for 1 h in air atmosphere for removal of residual surface carbon. Additionally, reference samples of pure ZnO and carbon graphite were also prepared. A single batch was used for carbon doped ZnO samples to guarantee identical synthesis conditions, while ZnO and pure graphite were separately annealed to avoid any contamination. Finally, the pellets were grounded by mortar and pestle until homogeneous powders were obtained for characterization.

X-ray diffraction (XRD) patterns were collected at RT using a Phillips X'Pert X-ray diffractometer with a Cu-Kα source (λ= 1.5406 Å) in Bragg-Brentano geometry. The XRD patterns were fitted using the Rietveld method to obtain crystalline cell parameters. Real carbon and oxygen content were measured using an Elemental Analyzer (CHNS/O) Leco Truspec Micro, through ASTM D5373-08 test method. The Fourier transform infrared (FTIR) spectra of the samples were recorded using a FTIR Bruker tensor 27 Spectrophotometer, using the KBr pellet technique, with an experimental resolution of 4 cm^{-1} approximately. Micro-Raman measurements at RT were performed on a Horiba Jobin–Yvon LabRam HR system. Raman scattering was excited with the 633 nm line of a He–Ne laser source. A CCD camera was used as a detector and for collecting the laser light with a spatial resolution of 2-4 μm. RT optical absorption spectra in the ultraviolet and

visible light wavelength were measured using an Evolution 600 UV–Vis spectrophotometer (Thermo Scientific) fitted with an integrating sphere diffuse reflectance accessory. The XPS analyses were carried out with a Kratos Axis Ultra spectrometer using a monochromatic Al-Kα X-ray source (1486.7 eV) with an analysis area of 300 x 700 microns. The high resolution core level photoemission spectra were collected using a pass energy of 40 eV, whereas for survey scans pass energy was of 160 eV. The charge-shifted spectra were corrected using the adventitious C1s photoelectron signal at 284.8 eV. The overlapped bands of XPS spectra were deconvoluted using XPS PEAK41 software. The magnetic properties of the samples were studied using a PPMS-Physical Property Measurement System-, Model 6000. The measurements were carried out as a function of applied magnetic field (± 0.5 T) and as a function of temperature (5-300 K). The samples were tightly packed into a clear plastic sample holder and then mounted vertically. Utmost care was taken to avoid contacting the samples with anything that could be a possible source of magnetic contamination, such as stainless steel tweezers or blue pens.

3. RESULTS

3.1 ***X-ray diffraction***: Refinement of the XRD patterns using the Rietveld method for undoped ZnO and carbon doped ZnO samples for various carbon nominal concentrations are shown in Figure 1. Within the sensitivity of XRD, all the diffractions peaks can be indexed to the wurtzite structure of ZnO phase. However, a small shoulder located at 26.8^{o} was observed in the XRD patterns with $x \geq 0.05$ when the y-axis is plotted in logarithmic scale and it could be correlated with traces of free carbon. Although the XRD line broadening is not reliable, yielding large errors in average crystallite size (D_V), the undoped and carbon doped ZnO powders can be considered as bulk materials, with range values of D_V between 1–2 μm. The lattice parameters derived from the fitting of the XRD

data of all the samples are summarized in Table 1. The *a* and *c* lattice parameters, the lattice volumes and *L* (Zn–O bond length along the *c* direction),[38] gradually increase as carbon doping concentration *x* increases to 0.03 and then decreases and becomes constant with the increment the doping concentration. On the other hand, *c/a* and *R* (distortion degree)[39] parameters remain almost constant in the whole range of doping. From Table 1 it is evident that the structural change in carbon doped ZnO is different below and above the doping concentration of 3 mol %. The ionic radii of O^{2-}, C^{4-} and Zn^{2+} in a tetrahedral environment are 1.40, 2.60 and 0.60 Å respectively.[26,40] Obviously the radius of dopant ion C^{4-} is higher than that of host O^{2-} and Zn^{2+} ions. Therefore, it is expected that substitution of O by carbon (C_O) and/or Zn by carbon atoms (C_{Zn}) will expand the lattice. The observed increment of the lattice parameters with increasing carbon concentration up to 3 mol % could be due to the partial substitution of carbon atoms in ZnO matrix, replacing either oxygen and/or zinc positions, although the presence of interstitial carbon could also influence in the expansion of the ZnO lattice.[26] This phenomenon brings about structural distortion in ZnO and changes in both the O–Zn–O bond lengths and the Zn–O–Zn bond angles. Additionally, the variation in the O (*z*) positional parameter (see Table 1) might be strong proof that structural changes have occurred when carbons atoms are introduced into the ZnO matrix. Above $x = 0.03$, the observed decrease in the lattice parameters could suggest the presence of high concentrations of free graphitic carbon.

From the results of elemental composition analysis, (see Table 1) we observed that with increasing carbon content in ZnO, the oxygen content decreases, which could indicate a systematic deficiency of oxygen in the system upon increasing the carbon doping. In fact, it is well known that synthesis in an argon atmosphere in doped ZnO could increase the formation of V_O in the system which lead

to its non-stoichiometric state.[41] Interestingly, in all of the carbon doped ZnO samples, the carbon percentage plus oxygen percentage does not vary significantly with increasing carbon content, thus obtaining a similar Zn content for these samples, but minor than that for the ideal wurzite ZnO. These results could additionally imply a possible zinc deficiency with the incorporation of carbon in the ZnO matrix.

These observations might reflect the effect of the partial C_O and/or C_{Zn} in ZnO. Such situation might rearrange of neighboring oxygen and zinc ions and thus, formation of V_O and or V_{Zn} could be required to maintain the system neutral. Therefore, a non-stoichiometric factor and defects induced by the incorporation of carbon atoms might contribute to the observed variation of the lattice parameters of ZnO.

3.2 ***Fourier transformed infrared spectroscopy***: Typical FTIR absorption spectra of pure ZnO and carbon doped ZnO samples are shown in Figure 2. For all samples a weak band near 3450 cm^{-1} and two strong absorption bands overlapping around 437 and 525 cm^{-1} were observed. The band at 3450 cm^{-1} belongs to stretching vibrations of hydroxyl groups corresponding to ambient water molecules absorbed on the surface of ZnO powders. The band around 437 cm^{-1} can be assigned to the antisymmetric stretching vibrations of O–Zn–O bonds in tetrahedral coordination,[42,43] and hence is sensitive to the sub-lattice disorder, while the band appearing around 525 cm^{-1} may be associated with oxygen deficiency and/or V_O in ZnO.[43,44] Closer inspection in the wavenumber range < 700 cm^{-1} indicates that the absorption band at 437 cm^{-1} is blue shifted, while the band located at 525 cm^{-1} decreases in intensity with increasing carbon concentration. The first vibrational change suggests that the O–Zn–O bond in ZnO structure is affected by the presence of carbon, while the

second one could be correlated to a reduction in the O/Zn ratio. The blue shift of the band located at 437 $cm^{-1}$with increasing carbon content could be related with the replacement of C_O into the ZnO structure. In fact, if carbon substitutes oxygen at their sites, then we expect changes both in the reduced masses and in the strengths of the chemical bonds, which affects the positions of the IR bands. The reduced mass of the Zn–O bond is greater than that of the Zn–C bond, therefore, the partial C_O should shift the IR band towards higher wavenumber, as it was indeed observed. On the other hand, the difference in the electronegativities for Zn and O are higher than that for Zn and carbon, which implies that the bonds change from more ionic (for Zn–O) to more covalent (for Zn–C) character, *i.e.* it becomes stronger with the C_O formation, again implying a shift toward higher wavenumbers, as it was observed. Therefore, these FTIR results may indicate that carbon atoms bring about structural changes in the ZnO structure. It is worth noting that in the FTIR spectra of carbon doped ZnO samples, very weak bands located at ~ 1390 and 1630 cm^{-1}, (orange circle), could indicate the presence of C–O and C=O bonds, respectively,[45] while residual bands centered at ~ 970 cm^{-1} (green circle), might be assigned to out of plane polarised C-O stretch.[46]

3.3 *Micro-Raman*: Micro-Raman scattering is a versatile technique for detecting the incorporation of dopants and the resulting defects and disorder in the host lattice. The RT micro-Raman spectra of undoped and carbon doped ZnO samples ranging from 50 to 700 cm^{-1} are shown in Figure 3. The observed phonon wavenumbers in the micro-Raman spectra of ZnO are consistent with previous studies.[47–49] The micro-Raman spectrum of pure ZnO is dominated by two intense and sharp E_2^{low} and E_2^{high} modes at 102 and 441 cm^{-1}, respectively. The peak that appears at 209 cm^{-1} is assigned to $2E_2^{\mathrm{low}}$, while the feature at 334 cm^{-1} has been assigned to second order scattering E_2^{high}-

E_2^{low}. The peak at 385 cm^{-1} can be assigned to the A_1(TO) mode and the weak peak located at 410 cm^{-1} represents the E_1(TO) mode.[47–50] Finally, the hump located at 483 cm^{-1} can be assigned to LA overtones along M-K point of the Brillouin zone and associated to a zone-boundary multi-phonon process of ZnO.[50–52] It is worth mentioning that the E_2^{low} mode, involves mainly Zn motion in sub-lattice, while the E_2^{high} mode mainly involves the vibration of the oxygen atoms.[48] From Figure 3 it can be seen that all peaks in carbon doped ZnO samples decrease in intensity in comparison to undoped ZnO sample, evidencing a gradual structural disorder in ZnO lattice with increasing carbon concentration. With increasing carbon content the E_2^{low} mode is shifted gradually to lower wave number reaching a minimum for x= 3% [(see the inset (a) of Figure 3] and then are shifted to higher wavenumber with further increase in the doping. This behavior is consistent with the results of Rietveld analysis obtained from the XRD pattern, which pointed out a different structural change in carbon doped ZnO samples below and above the nominal doping of 3 mol %, indicating a double regime in ZnO structure when carbon atoms are incorporated into the semiconductor. The first regime might reflect the formation of C–Zn–O bonds and the second one, might reflect the formation of C–Zn–C bonds, which could explain the weak collapse in lattice volume of ZnO structure. Indeed, this behavior can be compatible with an increase of disorder in ZnO structure, possibly indicating the formation of V_O, in agreement with the gradual decreasing of the oxygen percentage as pointed out in the elemental analysis. Additionally, from inset (b) of Figure 3, it can be seen that the intensity of the E_2^{high} mode gradually decreases up to 3 % and drastically decreases with further carbon doping. This behavior could indicate a substantial reduction of O–Zn–O bonds and higher formation of O–Zn–C or C–Zn–C bonds in the ZnO matrix from 3 mol % nominal doping upwards. It is important to note that A_1(TO), E_1(TO) modes and LA overtones seem to

disappear soon after 3%. These observations could indicate that with increasing carbon concentration the presence of defects (vacancies, interstitials and/or free graphitic carbon) in the ZnO structure, induced by non-uniform distribution of the carbon in ZnO matriz, could reduce the lattice symmetry, lift the Raman selection rule and therefore several phonon vibration modes which are originally in the perfect lattice of the wurzite structure become inactivates. The micro-Raman spectra in the range 1000-2000 cm^{-1} of pure and carbon doped ZnO samples are shown in Figure 4. The spectrum of graphite, prepared under similar conditions, is also included as a reference. In the Raman spectrum of pure ZnO we observed a weak peak at 1105 cm^{-1} and a broad and intense band at 1158 cm^{-1}. These bands are attributed to optical overtones and are associated with second order Raman active modes.[50] The former peak can be can be attributed to 2LO mode of ZnO, while the latter one contains contributions of $2A_1$(LO) and $2E_1$(LO) modes.[50,52] The Figure 4 shows that the peak located at 1105 cm^{-1} disappears, while the intensity of the band at 1158 cm^{-1} decreases and broadens as the carbon content increases, confirming that the O–Zn–O bond is seriously affected by doping. In the range 1400-1700 cm^{-1} (graphitic region) the peaks located at 1340 cm^{-1}, 1590 cm^{-1} and 1624 cm^{-1} are associated to the so-called *D, G* and *D'* bands[53,54] indicating the presence of free graphitic carbon in all of the carbon doped samples. The evolution in the intensity of *D* and *G* peaks can be ascribed to the change in the size of free nanocrystalline graphite.[53,55] Several other studies on carbon doped ZnO samples have also reported these similar graphite bands by using micro-Raman spectra.[21,30,31,45,55]

The techniques used so far probably suggest a partial C_O in the wurzite structure with the formation of intrinsic complex defects along with the presence of carbon free in all of the doped ZnO samples. The additional carbon atoms at concentrations beyond 3% could indicate that O–Zn–O bond is

seriously affected. This fact may be manifested in the reduction of lattice parameters in XRD patterns and the shifting toward higher wavenumbers in the micro-Raman spectra, when carbon concentration reaches 3 mol %, inactivating some vibrational modes in ZnO lattice. These observations reveal that the local symmetry in the carbon doped ZnO samples is different from that of the undoped one.

3.4 *Optical absorption*: Figure 5 (a) shows RT optical absorption spectra of pure ZnO as well for carbon doped ZnO samples in the range of 350–800 nm. All powders performed in a highly transparent mode in the visible region. The systematic variation in the drop of light absorption with increasing doping content could suggest that carbon atoms were incorporated into ZnO matrix. Diffuse reflectance spectra [see inset of Figure 5 (a)] suggest that the carbon doping does not change direct electron transition characteristics of ZnO. The carbon doped ZnO samples have lower reflectance than the pure ZnO sample which implies that these doped ZnO samples could benefit the photocatalytic applications of solar light for target reactions.[19,20,56–59] Based on the absorption spectra, the direct band gap can be estimated applying Kubelka–Munk rule by extrapolation of the linear portion to the zero in the plot of $(\alpha hv)^2$ against the photon energy hv as presented in Figure 5 (b).The dependence of the band gap (Eg) on carbon content is displayed in the inset of Figure 5 (b). It is observed that undoped ZnO sample shows an Eg value of ~3.31 eV and is slightly red shifted with increasing carbon concentration. In this work we have evidenced that most of the carbon atoms were not incorporated homogeneously in ZnO structure. Then, in this case, according to XRD results, the change in the band gap cannot be explained on the basis of the variation of the lattice parameters observed in the carbon doped ZnO samples. This gradual decrease in the band gap with increasing of carbon content may be mainly related to carbon atoms in the ZnO lattice. This situation

could promote and introduce impurity or defect levels, mainly V_O or V_{Zn} to the midgap of ZnO, modifying its band structure and thus narrowing the band gap.[19,44,60] The narrowing of the band gap of carbon doped ZnO samples, in comparison to pure ZnO, could also be related to interactions between the localized *p* electrons of the carbon ions, substituting O^{2-} ions and the 4s and 4p electrons of the host band of ZnO. This behavior may be similar to s, p–d exchange interaction between the band electrons and the localized d electrons of TM substituting metal ions in semiconductor oxides. These optical absorption results suggest that carbon doped ZnO powders may present a higher sensitivity to visible light activity than pure ZnO sample and therefore could be utilized for future photocatalytic applications.

3.5 ***X-Ray Photoelectron Spectroscopy*****:** Figure 6 shows survey scan of the XPS spectra of pure graphite, undoped ZnO and carbon doped ZnO samples for various doping concentrations. All of the observed peaks can be ascribed to Zn, O and C, along with their Auger peaks as labeled in Figure 6. No peaks belonging to the core of TM ions were observed within the detection limit of the technique. The energy dispersive X-Ray (EDX) results, obtained from SEM analysis (data not shown) in 3 and 5 mol % carbon doped ZnO samples revealed similar results as XPS, where TM were not evidenced, confirming that the samples are composed mainly of Zn, O and C.

The Zn 2p core electron XPS data of pure and carbon doped ZnO samples are displayed in Figure 7. A single component was necessary for fitting the spectrum of the pure ZnO sample. This signal centered at 1021.48 eV was attributed to Zn^{2+} ions tetrahedrally coordinated on the wurtzite structure surrounded by O^{2-} atoms. On the other hand, in carbon doped ZnO sample the introduction of a second component is observed, both visually and statistically, through deconvolution. If we consider the difference in the electronegativity of O (χO=3.44) and C (χC=2.55), this second

component shifted to higher energy centered at ~1022.23 eV could be related to Zn–oxy–carbide (Zn–O–C) bonds, due to the small difference in binding energy (BE) with the Zn–O–Zn peak (~0.7-0.8 eV).

Figure 8 shows the high resolution O 1s core level spectra of undoped and carbon doped ZnO samples. The O 1s peak of pure ZnO sample was deconvoluted into two components with BE of 530.17 eV and 532.06 eV respectively. The first component, at 530.17 eV, denoted O1, can be attributed to the O^{2-} ions in the hexagonal wurzite ZnO structure which are bound to Zn^{2+}, [60] while the second component might indicate the presence of loosely bound oxygen on the surface region of ZnO ascribed to the formation of −OH groups belonging to chemisorbed H_2O molecules.[4,44] The high resolution XPS scans of the O 1s core electron regions of 1, 3 and 5 % carbon doped ZnO samples were deconvoluted into four components. The first component is in the range of 530.15−530.10 eV corresponding to O^{2-} ions surrounded by Zn^{2+} atoms (O1). The two intermediate components centered around ~531.14 eV (O2) (blue shaded area) and 532.24 (O3) (red shaded area) are clearly evident through deconvolution. The former component (O2) can be deemed as primarily associated to Zn–O–C bonds,[19,22,44,45] while latter one has been assigned to C–O[33,44] and/or C–O–C bonds.[61] Although the O3 band is near to the component ascribed to chemisorbed −OH groups in undoped ZnO, it is noted that in carbon doped ZnO samples the intensity and the area under this peak is much higher and the full width at half maximum (FWHM) is lower in comparison to pure ZnO. Additionally FTIR did not reveal huge amount of such −OH groups. Then, is O3 component must be coming from the carbon doping and may be related with C3 peak (see below for the C 1s core level). Finally, the peak in the range of 533.00−530.30 eV denoted O4, may be assigned to COOR or COOH groups surface contamination. It is worth mentioning that the O2 component has

also been related to the variations in the concentration of V_O due to the presence of O^{2-} ions in the oxygen deficient regions within the matrix of ZnO, which may also indicate an higher environment with V_O when carbon atoms are introduced in the semiconductor.[22,60]

The C 1*s* core electron XPS data of carbon doped ZnO samples are displayed in Figure 9. The spectrum of graphite synthesized as reference material, is also included. The graphite spectrum showed two typical components corresponding to free graphitic carbon at 284.8 eV denoted as C1, and the adventitious contamination at 285.74 eV respectively. Additionally, it is observed the shake up π- π* satellite feature at 290.94 eV characteristic of aromatic rings. In carbon doped ZnO samples, the component indicated as C2 (blue shaded area) located around ~ 286.05 eV suggests the formation of Zn–O–C bonds,[19,22,44] while the component located at 287.02 eV (C3) has been assigned to O–C–O complex.[20,23,29,33,45] Interestingly, the intensity of C2 and C3 peaks in the carbon doped samples has a similar trend as the intensity of the O2 and O3 components of the O 1s core level. These XPS data reveals that the components O2-C2 and O3-C3 are strongly related, confirming the formation of Zn–O–C and O–C–O bonds. The peak located at 289.5 eV (C4) can be attributed to residual structural species of carbon in the form of COOR bonding and/or adsorption of surface CO_2.[19,23] Note that 1 % carbon doped ZnO samples show a weak peak appears with a BE of 283.68 eV, which is drastically increased with increasing carbon concentration to 5 %. This fifth component (C5) clearly suggests the presence of carbon atoms in carbide form, indicating the higher C_O in the ZnO structure *i.e.* the formation of C–Zn–C bonds. To the best of our knowledge, a similar isolated band of great intensity belonging to C–Zn–C bonds in carbon doped ZnO system has not yet been reported. With increasing carbon concentration, a slight shift to lower energy is observed

in this component, indicating a higher electronic density around Zn–C bond when the carbon content is lower.

To provide insight on the electronic structure in pure ZnO and carbon doped ZnO, valence band (VB) XPS spectra obtained from survey scan is shown in Figure 10. The peak at ~10.4 eV is attributed to the Zn 3d band, while the peak at ~5.7 eV mainly involves the O 2p orbitals and the part of O 2p orbitals hybridized with the Zn 4s and 4p ones.[62] The VB's width of carbon doped ZnO are greater in comparison to undoped ZnO, revealing its VB electrons are delocalised and more dispersive. It is observed that FWHM of the peak located at ~10.4 eV is higher for 5 % carbon ZnO sample. With partial C_O there is bonding of carbon with Zn atoms and the possibility of C2p–Zn3d hybridization. In this case, Figure 10 indicates that the increase of carbon concentration increases hybridization of energy levels, confirming the systematic C_O in the ZnO structure. On the other hand, the broader band around ~5.7 eV in carbon doped samples could also imply an additional hybridization of O 2p with Zn 4s/4p and/or C 2p states in these samples, indicating an alteration of local electronic structure around the oxygen atoms.

In summary, XPS results demonstrate that in all of the samples, there exist the substitution of carbon atoms at both Zn sites and O sites to form Zn–O–C and O–C–O bonds with the alteration of local electronic structure around the oxygen atoms along with the formation of O–Zn–C and C–Zn–C bonds. Beyond 3% doping, the higher formation of C–Zn–C bonds, could explain the changes in E_2^{high} mode observed in micro-Raman spectra, and XRD as mentioned above. Although our results cannot identify with clarity other defects more than *Vo* and Zn deficiency these XPS findings could

indicate the possibility formation of carbon related complex defects in the system (vacancies, interstitials) from the C_{Zn} and/or C_O into ZnO matrix.[21,22,59]

3.6 ***Magnetic Measurements*** The RT *M* vs *H* curves at RT of carbon doped ZnO samples consist mainly of a linear part due to paramagnetic (PM) contribution, and an weak, but no negligible open curve due to FM contribution (data not shown). Figure 11 shows the RT *M* vs *H* curves of carbon doped ZnO samples, where the linear component has been subtracted (M-χ_p vs H) to illustrate the actual M_s and coercive field. Open and symmetric hysteresis loops are observed in the samples with 1 and 3 mol % carbon content revealing FM features, which decrease substantially with further increase in the doping, as shown in lower inset of Figure 11. The pure ZnO sample shows diamagnetic behavior, while pure graphite used as target shows PM behavior (shown in the upper inset of Figure 11). The PM behavior of pure graphite has been ascribed to a disordered mixture of sp^2-sp^3 bonds resulting in a antiferromagnetic (AFM) interaction spins from π -electrons originated at the edges of graphite layers.[63] In our case, this behavior could be attributed to disordered graphitic carbon originated of the preparation method. In carbon doped ZnO samples, the magnetization values increases rapidly with the increase of carbon content up to 3 % and then tends to decrease abruptly as doping increases. The M_s obtained at 300 K in this work (highest value of 2.3 memu/g for 3 mol % carbon) are comparable to those reported by Ye *et al.*[30] in carbon doped ZnO powders, but smaller than those found by Mishra *et al.*,[22] as well as to those reported for carbon doped ZnO thin films and theoretical values.[21,26] These results are similar to those found by Zhou *et al.*[26] in carbon-implanted ZnO films by PLD, where the similar value of M_s increases and then decreases with increasing carbon concentration. It is worth recalling that Nayak *et al.*[35] predicted based on

first-principles studies that a carbon concentration between 2% and 6% should be optimal to achieve d^0 ferromagnetism in carbon doped ZnO.

Figure 12 shows ZFC and FC curves for 3% carbon doped ZnO samples. It is noted that blocking temperature or spin glass behavior was not observed. Therefore, this *M* vs *T* curve along with *M* vs *H* hysteresis loop indicated the absence of TM clusters or superparamagnetic behavior, confirming that the carbon doping encourages the formation of the RTFM observed and is not related with any other hidden magnetic impurities. This *M* vs *T* curves does not fit the modified Curie-Weiss law. Then, the curve was fitted following the modified Curie-Weiss law, $\chi=\chi_o+C/(T+\theta)$ where χ_o represents non-paramagnetic contributions, *C* is the Curie constant and θ is the Curie-Weiss temperature. It is observed that this equation fits the experimental data well. The fit derived values are shown in Figure 12. The positive value for χ_o and θ indicated the combination of FM and AFM components respectively in the sample. The PM component could be due to the presence of disorder layer of graphitic carbon[63] into ZnO semiconductor, while the FM contribution is discussed below.

4. DISCUSSION

The main data collected using the various techniques suggest that the structural changes in carbon doped ZnO samples are different below and above the nominal 3 mol % carbon concentration. It is observed that increasing carbon doping in ZnO structure brings about a gradual structural modification in the ZnO lattice, primarily allowing for the formation of Zn–O–C and O–C–O bonds, along with intrinsic defects, mainly, V_O and Zn deficiency in the ZnO matrix. In all of the samples

the formation of O–Zn–C bonds in the carbide state are visible. With further increases in the doping above 5 mol % a noticeable increase in this bond C–Zn (C–Zn–C) is observed. Also, free graphitic carbon is present and the possibility formation of other defects that involve the partial C_{Zn} and C_O cannot be ruled out.

Identifying the source of the magnetic moments and their exchange interactions in carbon doped ZnO are two questions not simple at all, and in fact these are still matter of strong controversy in the literature at both the experimental and the theoretical points of view because they can be located at the defects, at the carbon atoms occupying oxygen sites or at the zinc sites. According to Pan *et al.*,[21] only carbon in the carbide state contributed to the magnetic moment and not the induced defects, suggesting the Zn–C system as the origin of the FM signal magnetism in carbon doped ZnO. They also pointed out that the ferromagnetism is attributed to the interaction of C 2p and O 2p (p-p interaction). This p-p interaction arising from the C_O in ZnO would generate holes in oxygen 2p states, leading to hole-mediated spin alignment of parent carbon atoms and thus indirect FM coupling between carbon atoms. The p-p interaction might be quite similar to p-d hybridization in TM's doped oxides. Ye *et al.*[31] and Li *et al.*[24] suggested that the FM properties in carbon doped ZnO can be attributed to the transfer of an electron from the d orbital of the Zn ion to the p orbital of the carbon ion, which results in the d orbital of Zn ions changing from d^{10} (completely filled) to d^9 (incompletely filled) state. Thus, the partial substitution of oxygen by carbon in ZnO produces bonding of carbon with Zn atoms producing C 2p and Zn 3d hybridization. Additionally, the generation of the donor defects such as *Vo* and/or Zn interstitial (Zn_i) are assumed to be two key factors in introducing magnetic ordering in carbon doped ZnO, which implicates that defects may induce RTFM into this system. On the similar way, Hsu *et al.*[34] reported that RTFM in carbon doped

ZnO would be mediated by defect promoted by carbon dopants and not to the incorporation of carbon at oxygen sites. Akbar *et al.*[33] mentioned that the ferromagnetism is not consistent with the models, which assume that it is originates from the substitution of carbon atoms for oxygen and with holes as the mediators of ferromagnetism. Therefore, they suggested that the ferromagnetism is another example of defect induced where the partial C_{Zn} leads to the stabilization of such defects that are FM. V_{Zn} are very likely a candidate for such defects that they have proposed as leading to the stabilization of RTFM in carbon doped ZnO. Similarly, Li *et al.*[24] proposed from experimental studies that both a certain number of donor defects such as V_O or/and Zn_i and the net spin at Zn ions caused by substitution of oxygen by carbon as the origin of the magnetic moment. Mishra *et al.*[22] pointed out that intrinsic defects may be responsible of the FM signature in carbon doped ZnO along with the development of Zn-oxy-carbon clusters. Ye *et al.*[30] suggested that the FM property of carbon doped ZnO powders is a result of C_O. When V_O are present in the ZnO lattice, there is a reduction of magnetic moment, where carbon-carbon distance could tune the FM in carbon doped ZnO powders. Furthermore, Nayak *et al.*[35] used first principles studies and found that the non-spin polarized C_{Zn} impurity is, under almost all conditions thermodynamically, more stable than the C_O impurity with the exception of very oxygen-poor and carbon rich conditions. This explains the experimental difficulties in sample preparation in order to realize d^0 ferromagnetism in carbon doped ZnO. They attributed it to the anisotropy of the dispersion of carbon impurity bands near the Fermi level, due to C_O impurities in ZnO, as the source of layered ferromagnetism. From their calculations, they derive that a carbon concentration between 2% and 6% should be optimal to achieve d^0 ferromagnetism in this system. Theoretical work carried out through spin-polarized electronic structure calculations performed by Nagare *et al.*[36], argued that connecting two carbon atoms via the zinc-oxygen network (C–Zn–O–C bond) is a significant factor favoring the FM

coupling in carbon-substituted Zn_nO_n (n = 3-10, 12) clusters. They proposed that the hybridization of zinc 4s with carbon 2p and oxygen 2p orbitals in carbon doped ZnO system play a crucial role in the FM interaction in carbon doped ZnO. Also, they theoretically showed that the oxygen ion that is connected with Zn and carbon ions (Zn–O–C) in ZnO crystal lattice is a crucial element in the formation of long-range magnetic interactions. All systems with two carbon impurities show FM interaction, except when carbon atoms share the same zinc atom as the nearest neighbor. They concluded that AFM coupling is favored if carbon atoms get substituted on sites adjacent to zinc (C–Zn–C). Finally, Subramanian *et al.*[32] reported from their experimental studies in carbon doped ZnO thin films, reported that C_O is the main source of magnetism. The long-range magnetic interactions at RT is achieved by the charge transfer between Zn 4s and C 2p orbitals along with the carbon–carbon interaction through oxygen ions. The zinc and oxygen related defects in carbon doped ZnO prevent the existence of hybridization between Zn 4s and C 2p and the formation of C–O bonds respectively and therefore there is absence of long range magnetic interaction in C–ZnO resulting in the nonexistence of magnetic moment around carbon. Then, they proposed that the defects are not responsible for the origin of RTFM and rather than is due to the intrinsic FM property.

Our experimental results may suggest that V_O, V_{Zn} and C_{Zn} defects do not have a crucial role in the FM signal. Our data confirm the presence of oxygen deficiency, which can be related with the formation of V_O. We expect that V_O could partially explain the continuous reduction in the E_g with increasing carbon content. But E_g does not show the same behavior as M_s. On the other hand, we found from elemental analysis that the Zn content in the carbon doped ZnO samples is slightly lower in comparison to the undoped ZnO sample, and that it remains reasonably constant with increasing carbon content in the samples. This data may suggest that the lower Zn content could be

related to the formation of C_{Zn}, V_{Zn} or both, but again the concentration of these defects remain constant for all carbon doped samples. Therefore, it is suggested that V_{O}, V_{Zn} and C_{Zn} cannot explain the FM signal. We have found a XPS peak with a BE of 283.68 eV in the C 1s core electron XPS, which drastically increases with increasing carbon content up to 5 %. This component clearly indicates the partial C_O in the ZnO structure. Here, it is important to mention that according to Nayak *et al*.[35] C_O can be stabilized under O poor and C rich conditions. And we prepared our samples under argon atmosphere and in the presence of carbon, therefore satisfying the experimental conditions required for the stabilization of C_O. Our experimental results agree with the theoretical studies reported by different groups point that the main magnetic source is neither zinc nor oxygen, but it is C_O the most probable source of the magnetic moment in our samples.[21,32,35,36]

We found that M_s increases with carbon up to 3 mol %, then decreases with further carbon content. Unit cell and volume parameters behaves similarly as M_s vs carbon. Also, the position of the E_2^{low} Raman band (102 cm^{-1}), associated to Zn vibrations and the formation of O–Zn–C and C–Zn–C bonds, behaves similarly as M_s. Next, the intensity of the O 2p hybridized Zn 4s and 4p (BE of 5 eV) from the valence band XPS spectra behaves similarly as M_s. Now, the intensity of the XPS peak with BE of 283 eV increases with carbon content up to 3 mol % carbon, but from this value onwards, it increases more abruptly. This behavior is similar to the intensity of the of the E_2^{high} Raman band (440 cm^{-1}), which decreases continuously as carbon increases, but it decreases more abruptly for 5 mol % onwards (related with the formation of C–Zn–C bonds). Then, the higher formation of C–Zn–C bonds seems to decrease the resultant magnetization giving rise to AFM interactions.

According to XPS the magnetic behavior in 1 and 3 % carbon doped ZnO samples could be associated with O2-C2 and O3-C3 peaks, (Zn–O–C and O–C–O bonds), along with an appropriate amount of O–Zn–C bonds. VB results indirectly indicate an alteration of local electronic structure around the oxygen, then, oxygen atoms probably play a crucial role in the magnetic properties of these materials. Thus, we deduce that the distributions of carbon as well as the chemical involvement in ZnO structure *i.e*. Zn–O–C, O–C–O and O–Zn–C bonds are important factors influencing the FM properties of these samples where oxygen atoms could mediate the long range magnetic. Our results seem to be in agreement with theoretical studies of Nagare *et al.*[36] where two carbon atoms bound to the same zinc atom as nearest neighbor encourage the AFM and that connecting two carbon atoms via the zinc-oxygen (C–Zn–O–C) favoring the FM coupling state. We propose that possibly the most appropriate model for explaining our experimental results are that the magnetic moments are located at the carbon atoms occupying the oxygen sites due to the charge transfer between Zn 4s and C 2p orbitals, (s–p hybridization formed by Zn 4s and C 2p orbitals) and that the exchange interactions between these magnetic carbon atoms are mediated by oxygens (p–p hybridization formed by O 2p and C 2p orbitals). These findings are in agreement with recently experimental results reported by D. Ngo *et al*.[64] from a local structure study of C-doped ZnO@ nanopaerticles. According to Nagare *et al.*[36] the FM interaction is mediated by oxygen, via π as well as σ bonds formed out of p electrons of carbon and oxygen. In this way, if there is an excess of C–Zn–C bonds the hybridization of zinc 4s with carbon 2p and oxygen 2p orbitals and O–C–O bound not take place and, thus, the FM signal is reduced.

5 CONCLUSIONS

We experimentally investigated in detail the crystallographic, optical, electronic and magnetic properties of carbon doped ZnO powders. XRD showed that the samples have a homogeneous hexagonal wurtzite crystal structure and along with micro-Raman results indicated different structural changes in ZnO below and above 3 mol % carbon doping. Elemental analysis evidenced oxygen and zinc deficiency in ZnO structure. Carbon incorporation in the ZnO structure slightly decreases the E_g of ZnO semiconductor. From FTIR it was observed that O–Zn–O bond is affected by carbon doping and XPS indicated the gradual formation of Zn–C bond with the presence of Zn–C–O and O–C–O bonds. RTFM was observed in carbon doped ZnO system even when most of the carbon was not incorporated at oxygen sites. Interestingly, the variation of M_s shows a similar trend as changes in Zn–C–O and O–C–O bond. These results suggested that the presence of C_O defects, with carbon atoms on an oxygen site, are the likely source of the magnetic moments, which may interact ferromagnetically via the mediation of oxygen atoms. The formation of C–Zn–C bonds encourage the AFM interaction and the formation of intrinsic defects induced by carbon atoms such as V_O, V_{Zn} and C_{Zn} do not have a crucial role in the FM signal.

ACKNOWLEDGMENTS

This study was supported in Colombia by CODI-University of Antioquia (Sustainability Program for the Solid State Group 2018-2019. Research at Boise State University was supported by NSF CBET 1134468, NSF EAGER DMR-1137419, and ARO W911NF-09-1-0051 grants. One of the authors, J.J. Beltrán would like to thank late Professor Alex Punnoose, he always guided me when I was at Boise. Thanks a lot for his valuable help, experience, knowledge and collaboration throughout my Professional development.

AUTHOR INFORMATION

Corresponding Author

* jailesbeltran@correo.unicordoba.edu.co, jjbj08@gmail.com

Author Contributions

All authors have given approval to the final version of the manuscript.

NOTES

The authors declare no competing financial interest.

References

1 T. Dietl, H. Ohno, F. Matsukura, J. Cibert and D. Ferrand, *Science*, 2000, **287**, 1019–1022.

2 X. Bie, C. Wang, H. Ehrenberg, Y. Wei, G. Chen, X. Meng, G. Zou and F. Du, *Solid State Sciences*, 2010, **12**, 1364–1367.

3 S. Kumar, Y. Kim, B. Koo, S. Gautam, K. Chae, R. Kumar and C. Lee, *Materials Letters*, 2009, **63**, 194–196.

4 D. E. Motaung, G. H. Mhlongo, S. S. Nkosi, G. F. Malgas, B. W. Mwakikunga, E. Coetsee, H. C. Swart, H. M. I. Abdallah, T. Moyo and S. S. Ray, *ACS applied materials & interfaces*, 2014, **6**, 8981–95.

5 X. Xu, C. Xu, J. Dai, J. Hu, F. Li and S. Zhang, *The Journal of Physical Chemistry C*, 2012, **116**, 8813–8818.

6 A. Sundaresan, R. Bhargavi, N. Rangarajan, U. Siddesh and C. Rao, *Physical Review B*, 2006, **74**, 161306.

7 J. Zhang, S. Xiong, X. Wu, A. Thurber, M. Jones, M. Gu, Z. Pan, D. A. Tenne, C. B. Hanna, Y. Du and A. Punnoose, *Physical Review B*, 2013, **88**, 085437.

8 M. A. Garcia, J. M. Merino, E. Fernández Pinel, A. Quesada, J. de la Venta, M. L. Ruíz González, G. R. Castro, P. Crespo, J. Llopis, J. M. González-Calbet and A. Hernando, *Nano letters*, 2007, **7**, 1489–94.

9 H. Peng, H. J. Xiang, S. H. Wei, S. S. Li, J. B. Xia and J. Li, *Physical Review Letters*, 2009, **102**, 017201.

10 X. G. Xu, H. L. Yang, Y. Wu, D. L. Zhang, S. Z. Wu, J. Miao, Y. Jiang, X. B. Qin, X. Z. Cao and B. Y. Wang, *Applied Physics Letters*, 2010, **97**, 232502.

11 M. H. Farooq, X.-G. Xu, H.-L. Yang, C.-J. Ran, J. Miao, M. Z. Iqbal and Y. Jiang, *Rare Metals*, 2013, **32**, 264–268.

12 S. Ghosh, G. G. Khan, B. Das and K. Mandal, *Journal of Applied Physics*, 2011, **109**, 123927.

13 S. Ullah Awan, S. K. Hasanain, M. F. Bertino and G. Hassnain Jaffari, *Journal of Applied Physics*, 2012, **112**, 103924.

14 Y. Liu, W. Zhou and P. Wu, *Journal of Alloys and Compounds*, 2014, **615**, 401–405.

15 Y. W. Ma, J. Ding, J. B. Yi, H. T. Zhang and C. M. Ng, *Journal of Applied Physics*, 2009, **105**, 07C503.

16 V. Bhosle and J. Narayan, *Applied Physics Letters*, 2008, **93**, 021912.

17 S. Chen, N. V. Medhekar, J. Garitaonandia and K. Suzuki, *Journal of Physical Chemistry C*, 2012, **116**, 8541–8547.

18 J. M. D. Coey, *Solid State Sciences*, 2005, **7**, 660–667.

19 X. Zhang, J. Qin, R. Hao, L. Wang, X. Shen, R. Yu, S. Limpanart, M. Ma and R. Liu, *The Journal of Physical Chemistry C*, 2015, **119**, 20544–20554.

20 D. E. Zhang, M. Y. Wang, J. J. Ma, G. Q. Han, S. A. Li, H. Zhao, B. Y. Zhao and Z. W. Tong, *Functional Materials Letters*, 2014, **07**, 1450026.

21 H. Pan, J. B. Yi, L. Shen, R. Q. Wu, J. H. Yang, J. Y. Lin, Y. P. Feng, J. Ding, L. H. Van and J. H. Yin, *Physical Review Letters*, 2007, **99**, 127201.

22 D. K. Mishra, J. Mohapatra, M. K. Sharma, R. Chattarjee, S. K. Singh, S. Varma, S. N. Behera, S. K. Nayak and P. Entel, *Journal of Magnetism and Magnetic Materials*, 2013, **329**, 146–152.

23 S. T. Tan, X. W. Sun, Z. G. Yu, P. Wu, G. Q. Lo and D. L. Kwong, *Applied Physics Letters*, 2007, **91**, 072101.

24 X. L. Li, J. F. Guo, Z. Y. Quan, X. H. Xu and G. A. Gehring, *IEEE Transactions on Magnetics*, 2010, **46**, 1382–1384.

25 T. S. Herng, S. P. Lau, C. S. Wei, L. Wang, B. C. Zhao, M. Tanemura and Y. Akaike, *Applied Physics Letters*, 2009, **95**.

26 S. Zhou, Q. Xu, K. Potzger, G. Talut, R. Grötzschel, J. Fassbender, M. Vinnichenko, J. Grenzer, M. Helm, H. Hochmuth, M. Lorenz, M. Grundmann and H. Schmidt, *Appl. Phys.*

Letters, 2008, **93**, 232507.

27 L. B. Shi, C. Y. Xu and H. K. Yuan, *Physica B: Condensed Matter*, 2011, **406**, 3187–3191.

28 K. Saravanan, G. Jayalakshmi, S. Chandra, B. K. Panigrahi, R. Krishnan, B. Sundaravel, S. Annapoorani, D. K. Shukla, P. Rajput and D. Kanjilal, *Physical Chemistry Chemical Physics*, 2017, **19**, 13316–13323.

29 N. D. Dung, C. T. Son, P. V. Loc, N. H. Cuong, P. T. Kien, P. T. Huy and N. N. Ha, *Journal of Alloys and Compounds*, 2016, **668**, 87–90.

30 X. J. Ye, C. S. Liu, W. Zhong, H. A. Song, C. T. Au and Y. W. Du, *Physics Letters A*, 2010, **374**, 496–500.

31 X. J. Ye, H. A. Song, W. Zhong, M. H. Xu, X. S. Qi, C. Q. Jin, Z. X. Yang, C. T. Au and Y. W. Du, *Journal of Physics D: Applied Physics*, 2008, **41**, 155005.

32 M. Subramanian, Y. Akaike, Y. Hayashi, M. Tanemura, H. Ebisu and D. L. S. Ping, *Physica Status Solidi (B) Basic Research*, 2012, **249**, 1254–1257.

33 S. Akbar, S. K. Hasanain, M. Abbas, S. Ozcan, B. Ali and S. I. Shah, *Solid State Communications*, 2011, **151**, 17–20.

34 H. S. Hsu, Y. Tung, Y. J. Chen, M. G. Chen, J. S. Lee and S. J. Sun, *Physica Status Solidi - Rapid Research Letters*, 2011, **5**, 447–449.

35 S. K. Nayak, M. E. Gruner, S. Sakong, S. Sil, P. Kratzer, S. N. Behera and P. Entel, *Physical Review B*, 2012, **86**, 054441.

36 B. J. Nagare, S. Chacko and D. G. Kanhere, *J. Phys. Chem. A*, 2009, **144**, 2689–2696.

37 C. Suk-Ho, L. Daeyoung, P. Joon Won, K. Dong Hak and L. Minchul, *Journal of the Korean Physical Society*, 2010, **57**, 1482.

38 H. Morkoç and Ü. Özgür, in *Zinc Oxide: Fundamentals, Materials and Device Technology*, ed. W. 2009 WILEY-VCH Verlag GmbH & Co. KGaA, 2009, pp. 1–76.

39 M. Gaudon, O. Toulemonde and A. Demourgues, *Inorganic chemistry*, 2007, **46**, 10996–1002.

40 (a) Shannon, R. D.; Prewitt, C. T. Effective Ionic Radii in Oxides and Fluorides. *Acta Crystallographic*, 1969, **B25**, 925−946.
(b) Shannon, R. D.Revised Effective Ionic Radii and Systematic Studies of Interatomic Distances in Halides and Chalcogenides. *Acta Crystallographic,* 1976, **A32**, 751−767.

41 A. Goktas, *Journal of Alloys and Compounds*, 2018, **735**, 2038–2045.

42 R. Elilarassi and G. Chandrasekaran, *Journal of Materials Science: Materials in Electronics*, 2012, **24**, 96–105.

43 G. Xiong, U. Pal, J. G. Serrano, K. B. Ucer and R. T. Williams, *Physica Status Solidi (C) Current Topics in Solid State Physics*, 2006, **3**, 3577–3581.

44 G. R. Dillip, A. N. Banerjee, V. C. Anitha, B. Deva Prasad Raju, S. W. Joo and B. K. Min, *ACS Applied Materials and Interfaces*, 2016, **8**, 5025–5039.

45 A. Tayyebi, T. Soltani, B. K. Lee, M. Outokesh and M. Tayebi, *Journal of Alloys and Compounds*, 2017, **723**, 1001–1010.

46 M. D. Frogley, C. Wang, G. Cinque and A. H. Barber, *Vibrational Spectroscopy*, 2014, **75**, 178–183.

47 K. A. Alim, V. A. Fonoberov, M. Shamsa and A. A. Balandin, *Journal of Applied Physics*, 2005, **97**, 124313.

48 T.-L. Phan, *New Physics: Sae Mulli*, 2012, **62**, 483.

49 D. Wang, Z. Q. Chen, D. D. Wang, N. Qi, J. Gong, C. Y. Cao and Z. Tang, *Journal of Applied Physics*, 2010, **107**, 023524.

50 R. Cuscó, E. Alarcón-Lladó, J. Ibáñez, L. Artús, J. Jiménez, B. Wang and M. J. Callahan, *Physical Review B*, 2007, **75**, 165202.

51 K. Samanta, P. Bhattacharya and R. S. Katiyar, *J. Appl. Phys.*, 2010, **108**, 1–5.

52 M. Schumm, *Doctoral dissertation*, 2008, 21–23.

53 M. A. Pimenta, G. Dresselhaus, M. S. Dresselhaus, L. G. Cançado, A. Jorio and R. Saito, *Physical chemistry chemical physics : PCCP*, 2007, **9**, 1276–1291.

54 H. Pardo, R. Faccio, F. M. Araújo-Moreira, O. F. De Lima and A. W. Mombrú, *Carbon*, 2006, **44**, 565–569.

55 H. Chen, S. Gu, W. Liu, S. Zhu and Y. Zheng, *Journal of Applied Physics*, 2008, **104**, 113511.

56 A. B. Lavand and Y. S. Malghe, *International Journal of Photochemistry*, 2015, **2015**, 1–9.

57 S. A. Ansari, S. G. Ansari, H. Foaud and M. H. Cho, *New Journal of Chemistry*, 2017, **41**, 9314–9320.

58 A. S. Alshammari, L. Chi, X. Chen, A. Bagabas, D. Kramer, A. Alromaeh and Z. Jiang, *RSC Advances*, 2015, **5**, 27690–27698.

59 S. Cho, J.-W. Jang, J. S. Lee and K.-H. Lee, *CrystEngComm*, 2010, **12**, 3929–3935.

60 J. P. Wang, Z. Y. Wang, B. B. Huang, Y. D. Ma, Y. Y. Liu, X. Y. Qin, X. Y. Zhang and Y. Dai, *Acs Applied Materials & Interfaces*, 2012, **4**, 4024–4030.

61 A. Omoike and J. Chorover, *Biomacromolecules* 2004, **5**, 1219-1230.

62 A. G. Joshi, S. Sahai, N. Gandhi, Y. G. R. Krishna and D. Haranath, *Applied Physics Letters*, 2010, **96**, 123102.

63 P. Esquinazi and R. Höhne, *Journal of Magnetism and Magnetic Materials*, 2005, **290–291 PA**, 20–27.

64 D. Ngo, L. T. Cuong, N. H. Cuong, C. T. Son and P. T. Huy, *Advanced Functional Materials*, 2018, **1704567**, 1–6.

TABLES

Table 1: Summary of the refined structural parameters of undoped ZnO and carbon doped ZnO samples along with elemental composition analysis data.

Parameter	ZnO	1 % carbon	3 % carbon	5 % carbon	8 % carbon	10 % carbon
a (Å)	3.2539	3.2550	3.2558	3.2546	3.2545	3.2546
c (Å)	5.2102	5.2118	5.2137	5.2112	5.211	5.2114
V (Å)^3	47.77	47.82	47.86	47.80	47.80	47.81
L (Å)	1.9875	1.9882	1.9886	1.9880	1.9879	1.9879
c/a	1.6012	1.6012	1.6014	1.6013	1.6012	1.6013
R	1.0199	1.0199	1.0198	1.0198	1.0199	1.0198
O(*z*)	0.3816	0.3801	0.3791	0.3766	0.3781	0.3762
χ^2	1.706	1.763	1.926	1.777	1.683	1.727
Elemental Composition Analysis						

Carbon content (%)	0 *	2.4	4.0	5.4	---	---
Oxygen content (%)	19.7*	17.8	16.1	15.0	---	---
Zn content (%)	80.3*	79.8	79.9	79.6	---	---

* Data obtained from ideal ZnO wurzite structure.

FIGURE CAPTIONS

Figure 1. Rietveld refinement analysis of XRD patterns of undoped and carbon doped ZnO samples. Semi solid spheres are experimental data, whereas solid lines represent the fit. The lines below represent the difference pattern. The goodness of fits is shown in Table 1.

Figure 2. FTIR spectra of pure ZnO and carbon doped ZnO samples. The inset shows the expanded region of the spectra in the range < 700 cm^{-1}.

Figure 3. Micro-Raman spectra of pure ZnO and carbon doped ZnO samples. The insets **(a)** and **(b)** shows the expanded region of the E_2^{low} and E_2^{high} modes of the spectra respectively.

Figure 4. Micro-Raman spectra of pure graphite, ZnO and carbon doped ZnO samples in the 1000-2000 cm^{-1} range.

Figure 5. (a) Absorption spectra and **(b)** plots of $(\alpha h\nu)^2$ against photon energy for undoped and carbon doped ZnO samples. The insets show the diffuse reflectance spectra and the variation of the calculated bandgap, following the Kubelka-Munk rule, with the nominal carbon doping concentration respectively.

Figure 6. Wide survey X-ray photoelectron spectra of pure graphite, undoped and carbon doped ZnO samples.

Figure 7. Zn 2p core-electron region spectra of undoped ZnO and carbon doped ZnO samples. The points are the experimental data, while the line represents the fit.

Figure 8. O 1s core-electron region spectra of undopd ZnO and carbon doped ZnO samples. The points are the experimental data, while the line represents the fit.

Figure 9. C 1*s* core-electron region spectra of graphite and carbon doped ZnO samples. The points are the experimental data, while the line represents the fit.

Figure 10. Valence-band XPS spectra obtained from survey scans of pure ZnO and carbon doped ZnO samples.

Figure 11. RT Magnetic hysteresis loops of carbon doped ZnO samples where the paramagnetic component has been subtracted. The upper inset shows hysteresis loops of undoped ZnO and pure graphitic carbon used as target, while the lower inset shows the low field region of all carbon doped ZnO samples.

Figure 12. *M* vs *T* without and with a constant applied field of 500 Oe for 3 mol % carbon doped ZnO. Open symbols represent FC, and solid symbols represent ZFC. Solid lines represent the theoretical simulations of the FC data using modified Curie−Weiss law. The fit derived values are also shown.

FIGURES

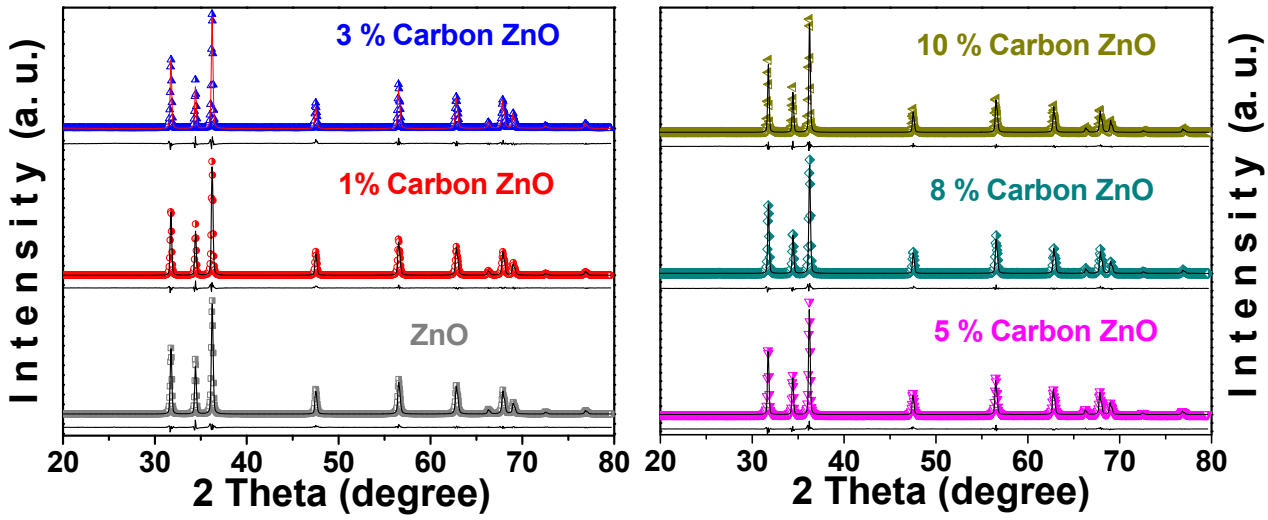

Figure 1. Rietveld refinement analysis of XRD patterns of undoped and carbon doped ZnO samples. Semi solid spheres are experimental data, whereas solid lines represent the fit. The lines below represent the difference pattern. The goodness of fits is shown in Table 1.

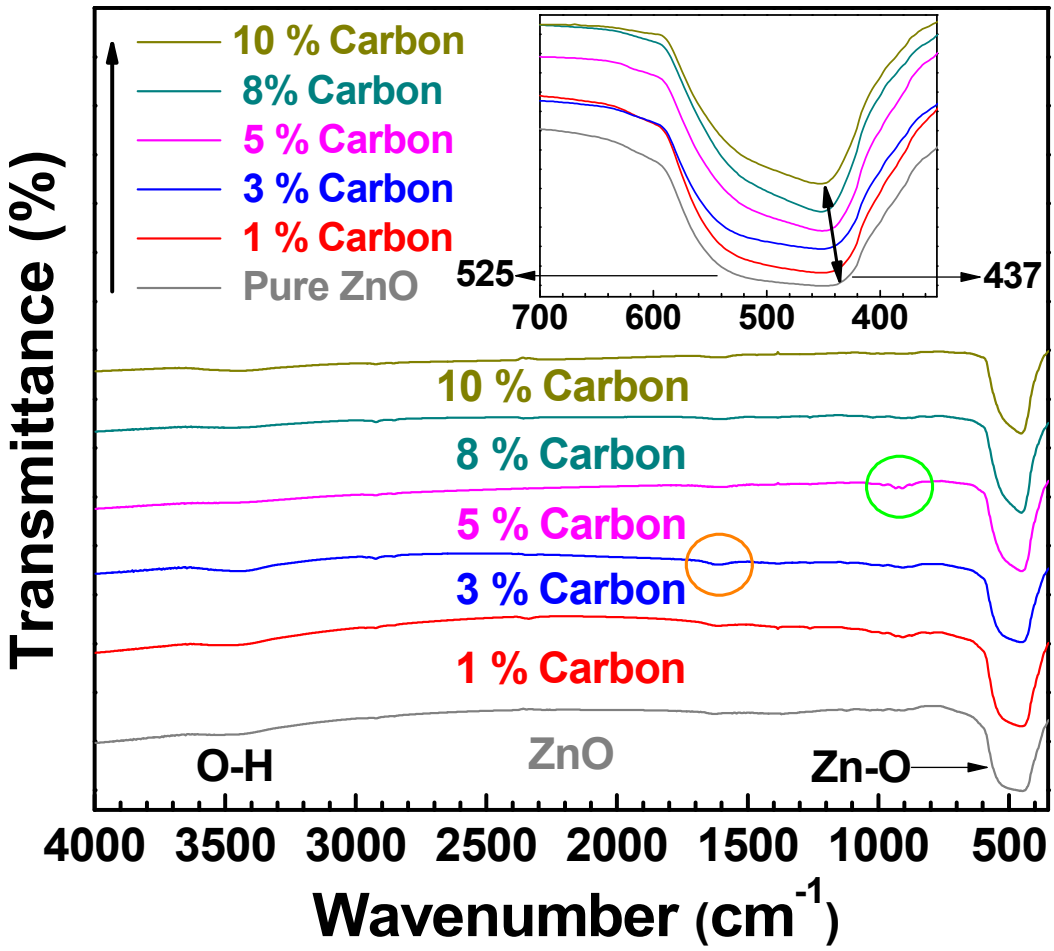

Figure 2. FTIR spectra of pure ZnO and carbon doped ZnO samples. The inset shows the expanded region of the spectra in the range < 700 cm^{-1}.

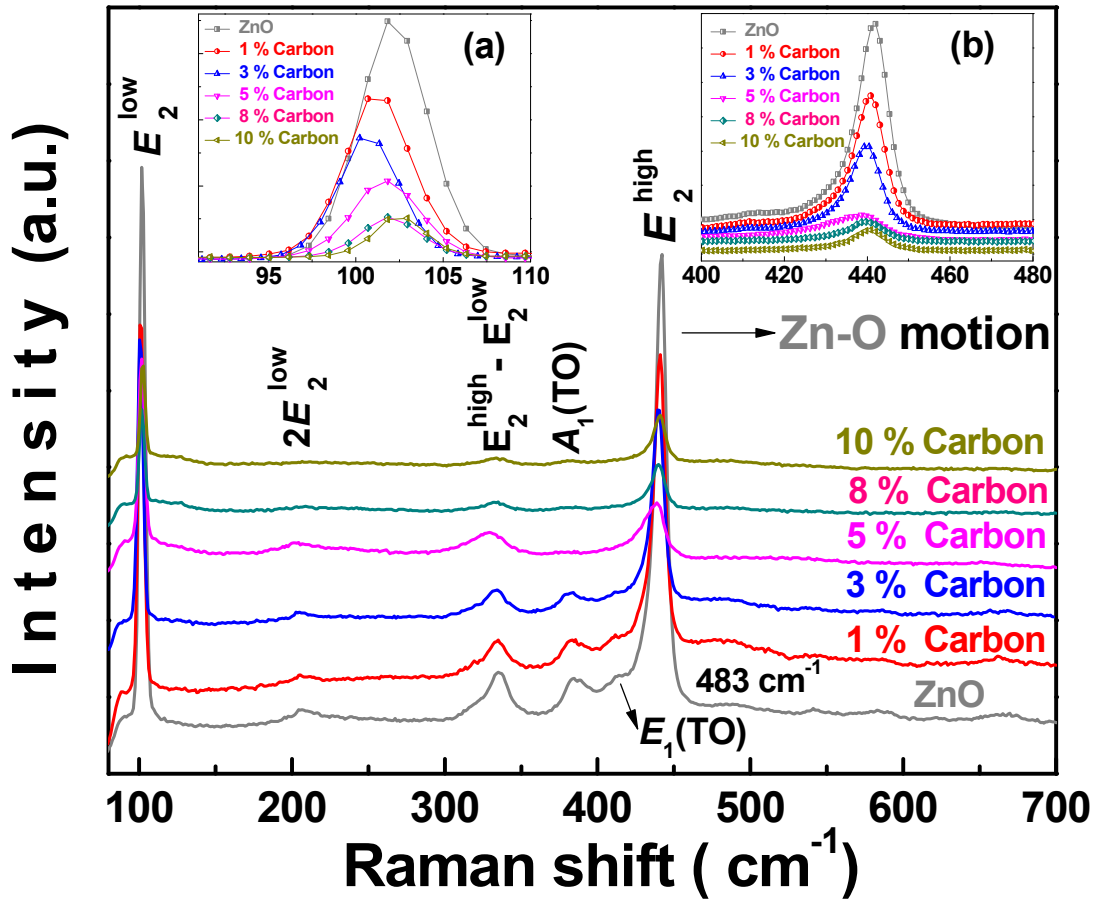

Figure 3. Micro-Raman spectra of pure ZnO and carbon doped ZnO samples. The insets **(a)** and **(b)** shows the expanded region of the $E_2^{low}$and E_2^{high}modes of the spectra respectively.

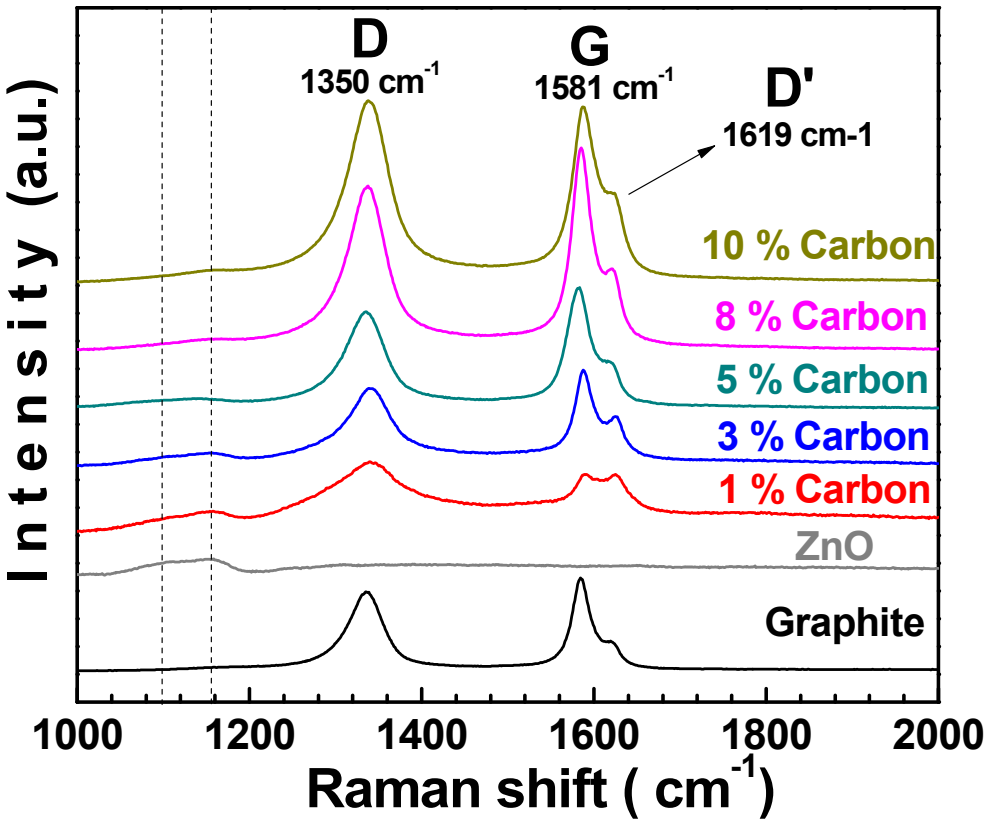

Figure 4. Micro-Raman spectra of pure graphite, ZnO and carbon doped ZnO samples in the 1000-2000 cm^{-1} range.

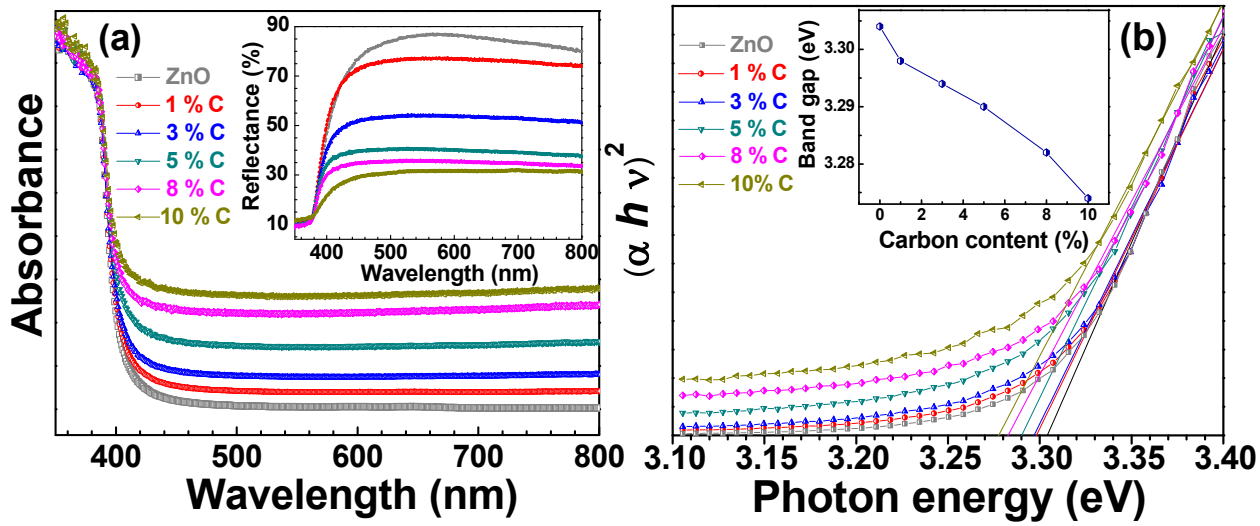

Figure 5. (a) Absorption spectra and **(b)** plots of $(\alpha h\nu)^2$ against photon energy for undoped and carbon doped ZnO samples. The insets show the diffuse reflectance spectra and the variation of the calculated bandgap, following the Kubelka-Munk rule, with the nominal carbon doping concentration respectively.

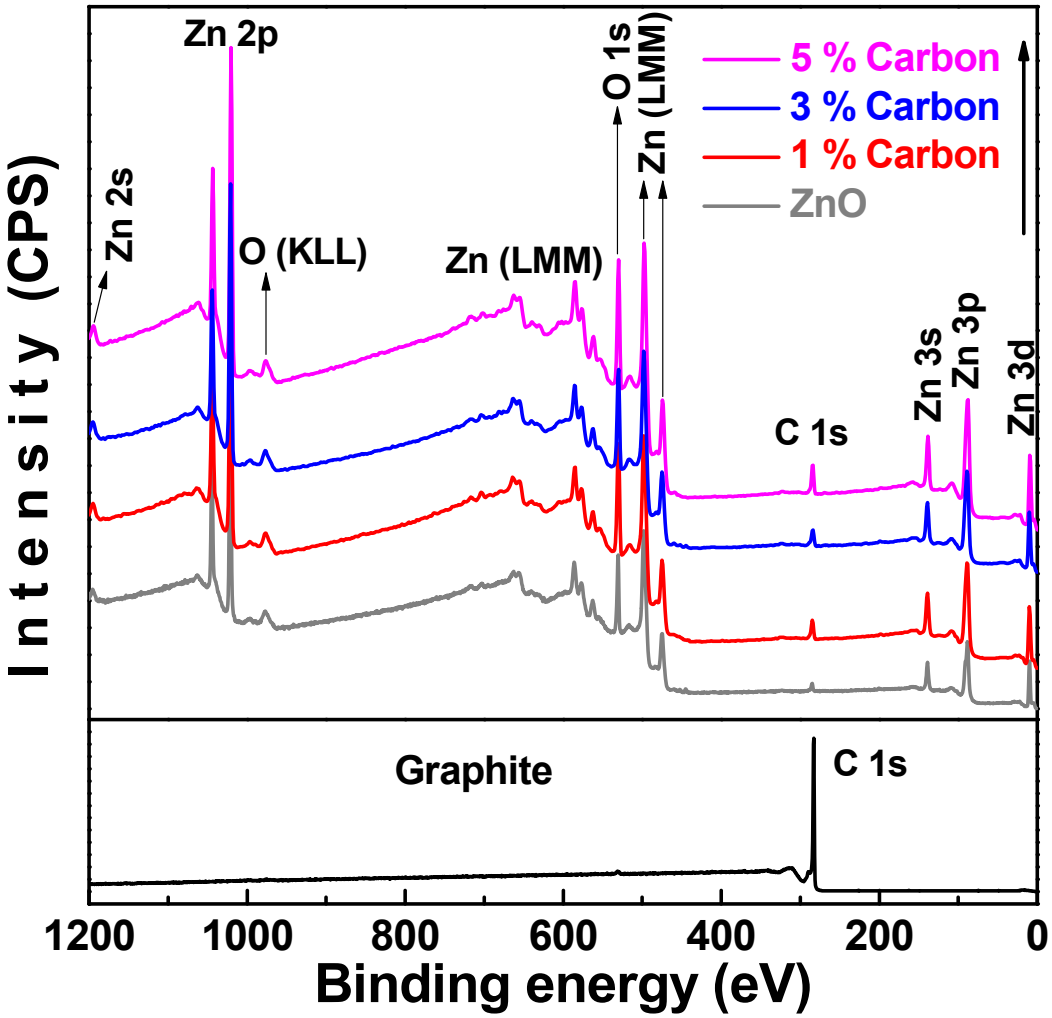

Figure 6. Wide survey X-ray photoelectron spectra of pure graphite, undoped and carbon doped ZnO samples.

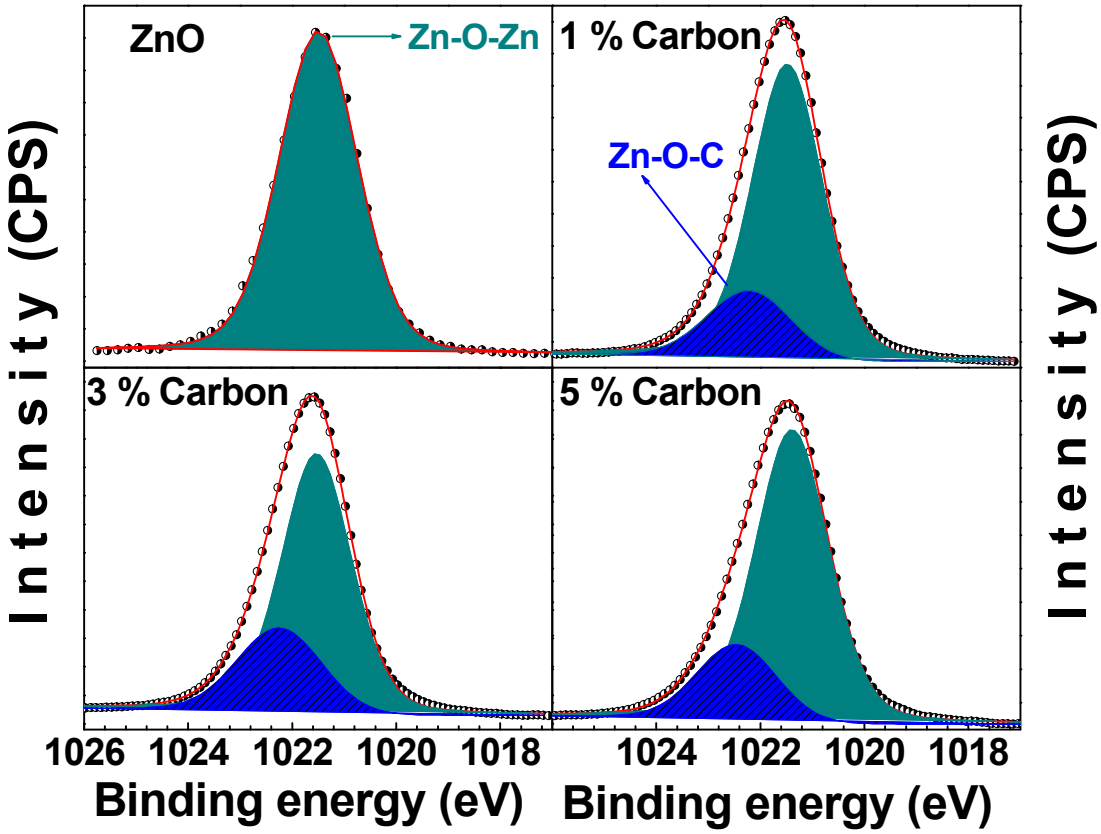

Figure 7. Zn 2p core-electron region spectra of undoped ZnO and carbon doped ZnO samples. The points are the experimental data, while the line represents the fit.

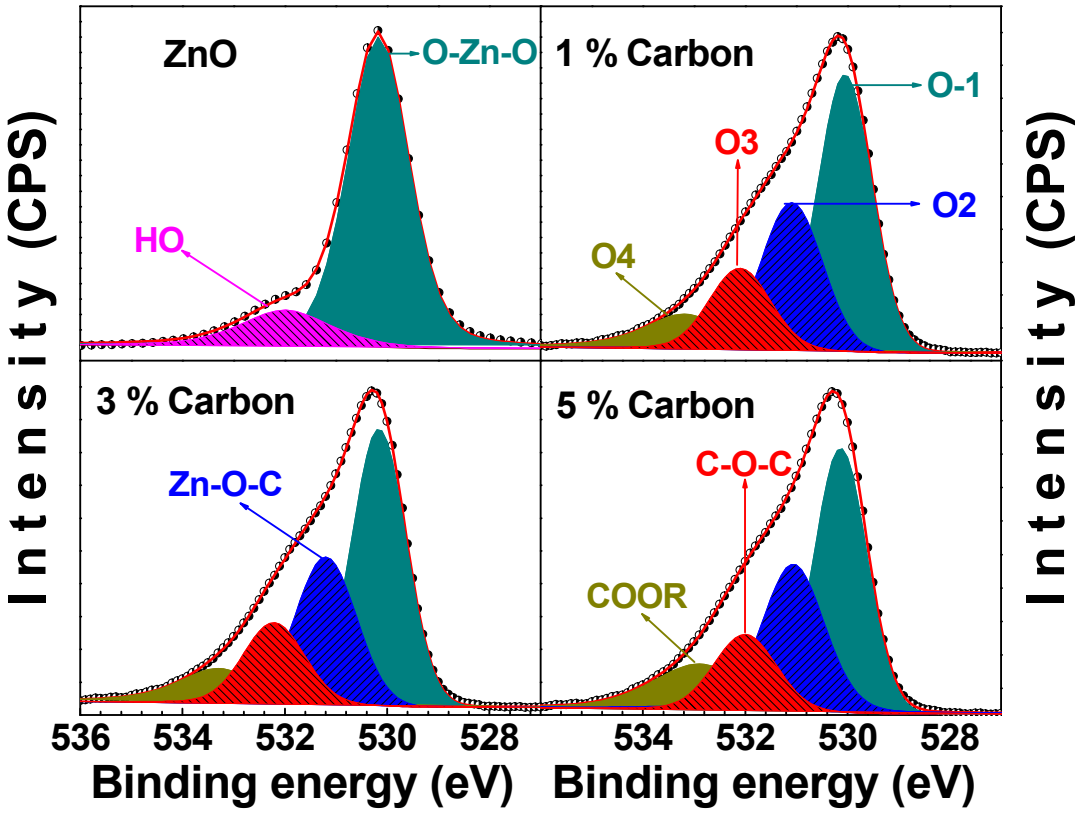

Figure 8. O 1s core-electron region spectra of undopd ZnO and carbon doped ZnO samples. The points are the experimental data, while the line represents the fit.

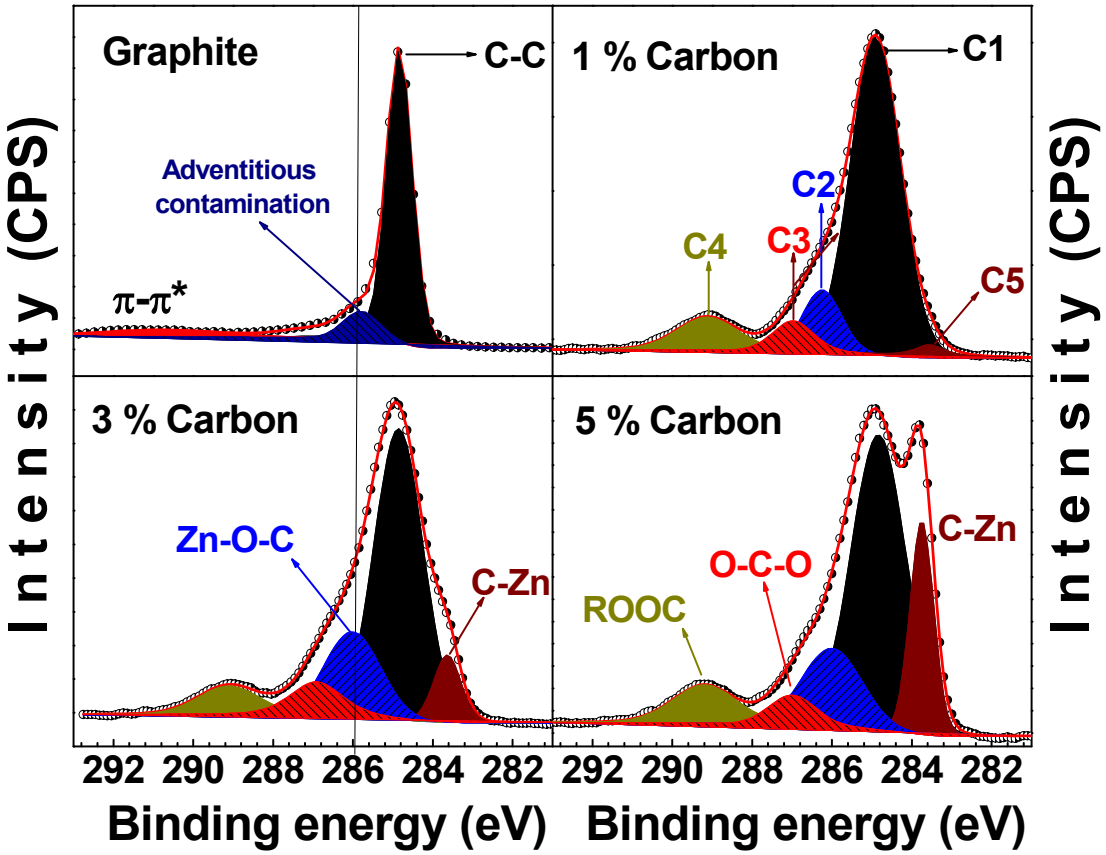

Figure 9. C 1*s* core-electron region spectra of graphite and carbon doped ZnO samples. The points are the experimental data, while the line represents the fit.

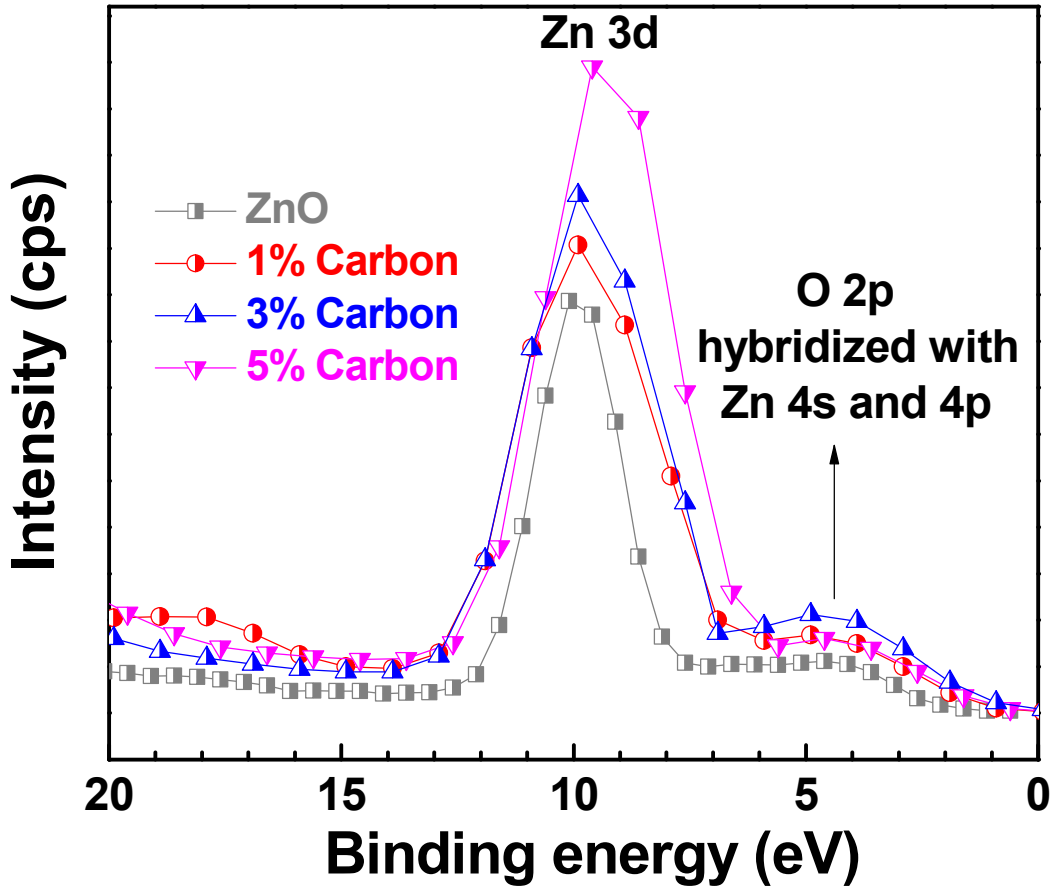

Figure 10. Valence band XPS spectra obtained from survey scans of pure ZnO and carbon doped ZnO samples.

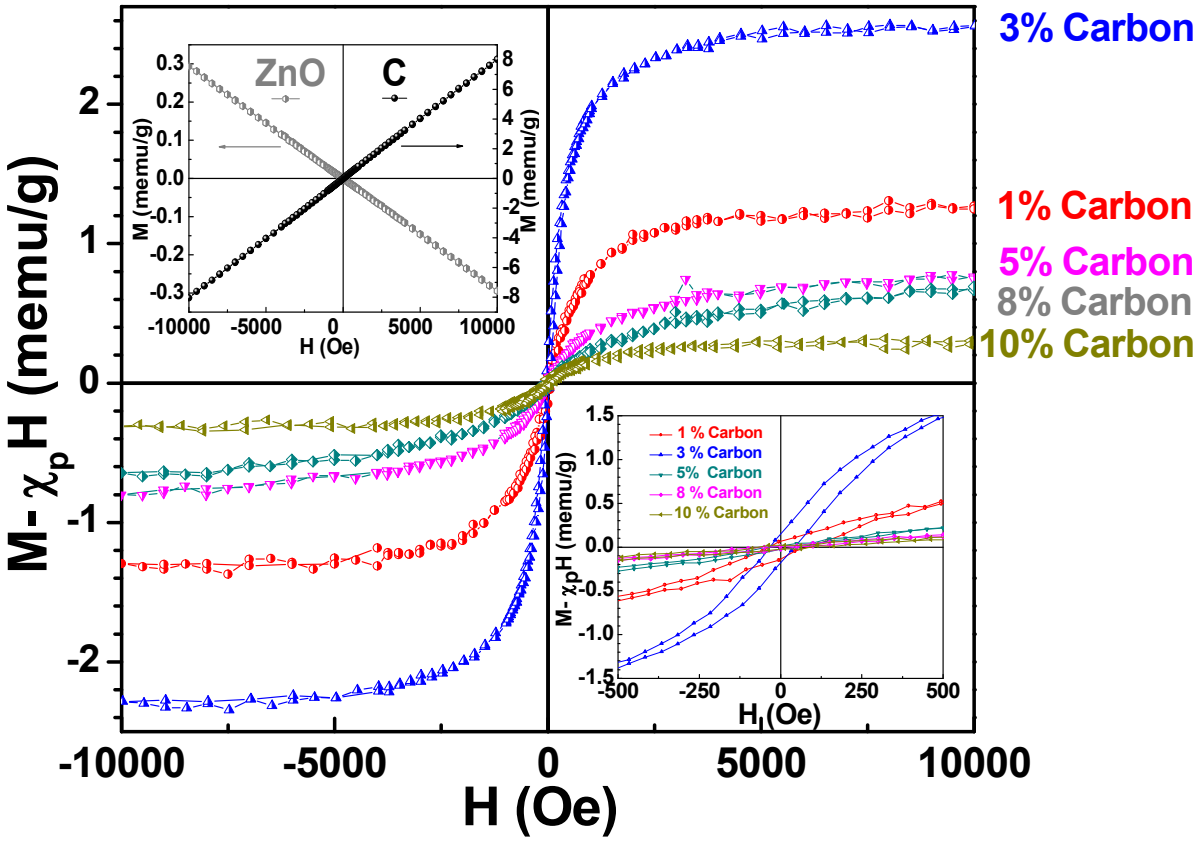

Figure 11. RT Magnetic hysteresis loops of carbon doped ZnO samples where the paramagnetic component has been subtracted. The upper inset shows hysteresis loops of undoped ZnO and pure graphitic carbon used as target, while the lower inset shows the low field region of all carbon doped ZnO samples

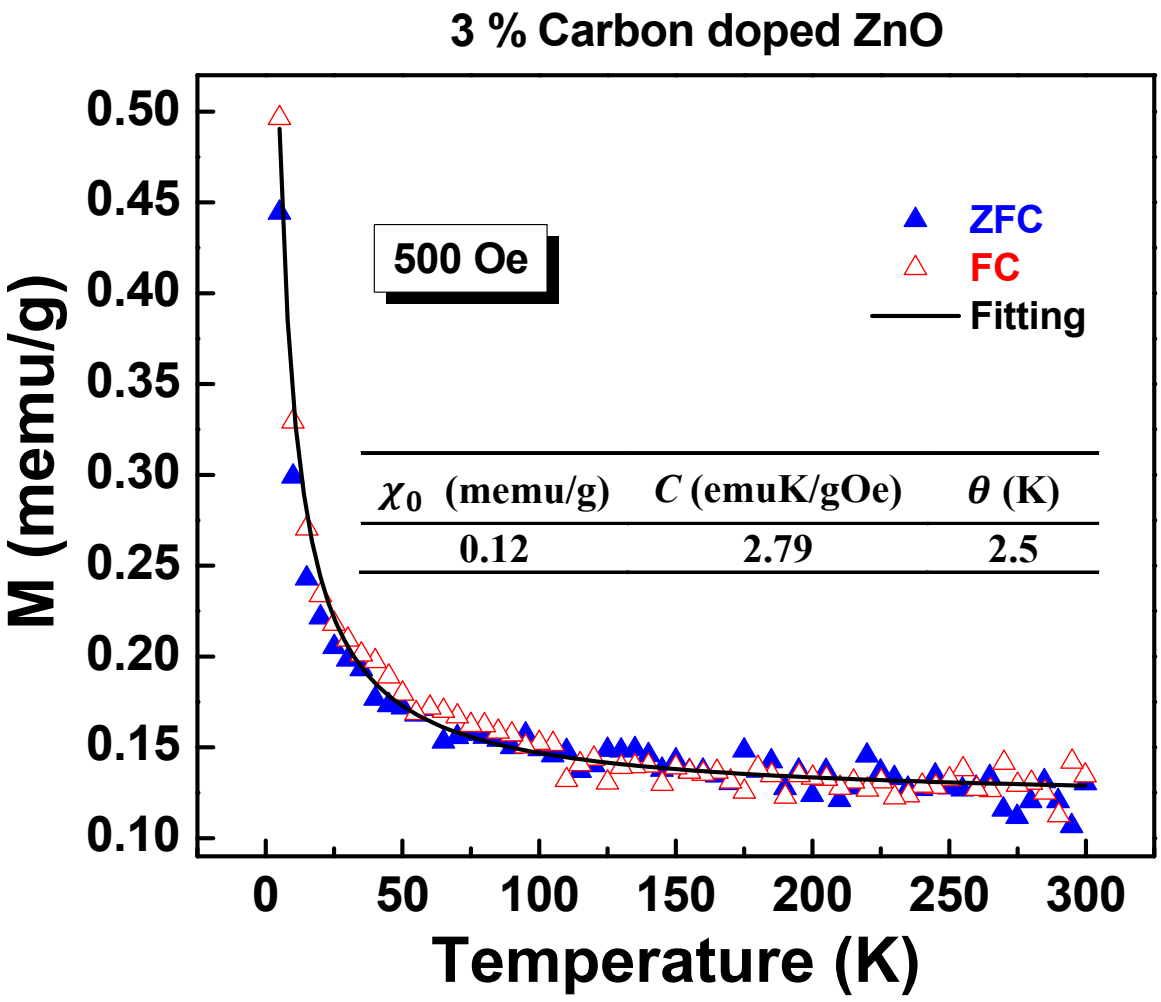

Figure 12. *M* vs *T* without and with a constant applied field of 500 Oe for 3 mol % carbon doped ZnO. Open symbols represent FC, and solid symbols represent ZFC. Solid lines represent the theoretical simulations of the FC data using modified Curie-Weiss law. The fit derived values are also shown.

TABLE OF CONTENTS ENTRY

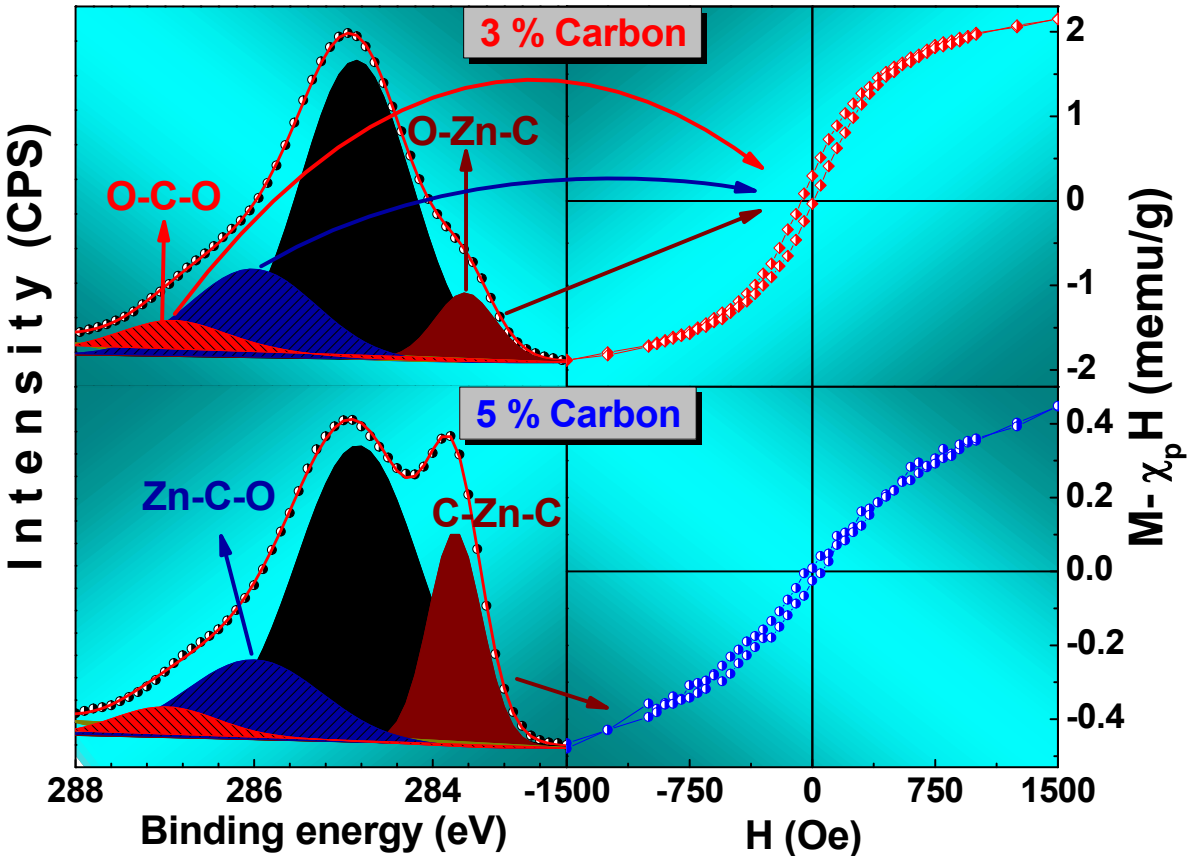

Carbon doped ZnO powders showed RTFM. Hybridization of Zn4s-C2p mediated by oxygens is the likely source of the FM behavior. C–Zn–C bonds encourage the AFM signal.